



Flow transitions in laminar Rayleigh–Bénard convection in a cubical cavity at moderate Rayleigh numbers

J. Pallares^{a,*}, F. X. Grau^a, Francesc Giralt^b

^a *Departament d'Enginyeria Mecànica*

^b *Departament d'Enginyeria Química, Escola Tècnica Superior d'Enginyeria Química, Universitat Rovira Virgili, Ctra. Salou s/n, 43006 Tarragona, Catalonia, Spain*

Received 23 January 1998; in final form 2 June 1998

Abstract

A three-dimensional numerical study of the natural convection in a cubical cavity heated from below is reported at moderate Rayleigh numbers for three Prandtl numbers $Pr = 0.71, 10$ and 130 . The six walls are considered rigid and immobile, with isothermal horizontal plates and adiabatic lateral walls. The Boussinesq approximation for the variation of physical properties is assumed. Seven different structures, four single roll-type, two four roll-type and a toroidal roll, and several flow transitions have been identified in the steady and laminar regime for $Ra \leq 6 \times 10^4$ and $Pr \leq 130$. Both, the dynamic and heat transfer characteristics of these seven structures are discussed. The effects of slightly changing the aspect ratio or tilting the cavity on the stability of the different structures are also analyzed. There is general agreement between the predicted average Nusselt number and available correlations for Rayleigh–Bénard convection in rectangular enclosures and between two horizontal plates. © 1998 Elsevier Science Ltd. All rights reserved.

Nomenclature

g gravitational acceleration [m s^{-2}]
 h heat transfer coefficient [$\text{W m}^{-2} \text{K}^{-1}$]
 k thermal conductivity [$\text{W m}^{-1} \text{K}^{-1}$]
 L reference length [m]
 Nu Nusselt number, hL/k
 P pressure [N m^{-2}]
 Pr Prandtl number, ν/α
 Ra Rayleigh number, $g\beta\Delta TL^3/\nu\alpha$
 S_{ij} strain tensor [s^{-2}]
 T temperature [K]
 t time [s]
 u, v, w velocity components [m s^{-1}]
 x, y, z Cartesian coordinates [m].

Greek symbols

α thermal diffusivity [$\text{m}^2 \text{s}^{-1}$]
 β thermal expansion coefficient [K^{-1}]
 δ thermal boundary layer thickness

δ_{ij} Kronecker delta
 γ angle of rotation around the x -coordinate
 ν kinematic viscosity [$\text{m}^2 \text{s}^{-1}$]
 Π second invariant of the velocity gradient tensor [s^{-2}],
 $S_{ij} S_{ji} + \Omega_{ij} \Omega_{ji}$
 Ω_{ij} rotation tensor [s^{-2}]
 Δ increment.

Superscripts and subscripts

* dimensionless quantity
C cold wall
c critical value
H hot wall
l local quality
s surface averaged quantity.

1. Introduction

Rayleigh–Bénard convection in a small aspect ratio enclosure heated from below is a convenient flow system to study transition from laminar to turbulent flow [1]. This system, which is governed by coupled non-linear partial differential equations for momentum and energy,

* Corresponding author. Fax: 977 55 96 91; E-mail: pallares@etseq.urv.es.

becomes unstable when the Rayleigh number or the dimensionless temperature difference between the bottom and top plates exceeds a given critical value. The first bifurcation corresponds to the transition from the conductive to the convective state and it is well documented in the literature for a variety of boundary conditions and values of the aspect ratio of the enclosures [2–5].

It is well known that for supercritical conditions a large variety of convective structures with differentiated topological and heat transfer characteristics can occur in a three dimensional enclosure. For example, Kessler [6] and Kirchartz and Oertel [7] have studied experimentally and numerically the three-dimensional structure of the non-linear thermal cellular convection in containers. However, an increase in Rayleigh number can produce substantial changes in the topology of the flow through mechanisms that are not well documented, especially for small enclosures where the influence of the lateral walls is suspected to dominate these evolutions. This information would also be useful to further investigate transition to turbulence [8].

Pallares et al. [9] carried out a preliminary study of the natural convection in the cubical cavity heated from below at Rayleigh numbers ($3.5 \times 10^3 \leq Ra \leq 10^4$) near to the transition from the conductive state regime and Prandtl number $Pr = 0.71$. For this geometry without preferred direction, they reported three different roll structures, named S1, S2, and S3, and a toroidal structure S4. These convective structures were stable and did not experience any subsequent transition for $Ra \leq 10^4$. Two of them, S1 and S3, had the axis of rotation parallel to two opposite vertical walls, while in S2 it was oriented towards two opposite vertical edges of the cube. Structures S1 and S2 were numerically predicted by Ozoe et al. [10]. The toroidal roll structure S4, with four ascending motions along the vertical edges and a single descending one at the centre, was reported previously by Hernández and Frederick [11]. This structure consists of an even combination of two x -rolls and two y -rolls, as suggested by Catton [3].

The aim of the present work is to study the formation, and the topological and heat transfer characteristics of other structures not reported previously for Rayleigh numbers up to 6×10^4 . The evolution of the structures and the transitions that occur between them as the Rayleigh number increases are characterized for three different Prandtl numbers, $Pr = 0.71, 10$ and 130 . The highest value $Pr = 130$ has been chosen because it is possible to carry out Rayleigh–Bénard convection experiments at moderate Rayleigh numbers using small cubical cavities ($L \approx 10^{-2}$ m) filled with silicone oil. The effects of changing the aspect ratio in one horizontal direction by 10% and in both horizontal directions by up to 20%, and of slightly tilting the cavity are analyzed. The heat transfer characteristics inside the cavity and at the top and bottom walls are also presented. The governing equa-

tions are described in Section 2 while the numerical scheme is discussed in Section 3. Finally, results are presented and discussed in Section 4.

2. Theoretical model

The geometry of the cubical cavity and the coordinate system are shown in Fig. 1. The two horizontal plates are isothermal and the four vertical walls are insulated. Compressibility effects, viscous dissipation and the variation of fluid properties with temperature have been neglected, with only the exception of the buoyancy term, for which the Boussinesq approximation has been used [12]. The reference scales for length, velocity, time and pressure are, respectively, $L, \alpha/L, L^2/\alpha$ and $\alpha^2\rho/L^2$, where L is the vertical dimension of the cube, α the thermal diffusivity and ρ the density of the fluid. Dimensionless temperatures have been defined with respect to the temperature difference between the hot and cold plates, $\Delta T = (T_H - T_C)$, according to $(T - T_O)/\Delta T$, where T_O is the mean temperature, $T_O = (T_H + T_C)/2$.

The governing transport equations in dimensionless form and in Cartesian coordinates are:

$$\frac{\partial u_i^*}{\partial x_j^*} = 0 \quad (1)$$

$$\frac{\partial u_i^*}{\partial t^*} + \frac{\partial(u_j^* u_i^*)}{\partial x_j^*} = -\frac{\partial P^*}{\partial x_i^*} + Pr \frac{\partial^2 u_i^*}{\partial x_j^* \partial x_j^*} + Ra Pr T^* \delta_{i3} \quad (2)$$

$$\frac{\partial T^*}{\partial t^*} + \frac{\partial(u_j^* T^*)}{\partial x_j^*} = \frac{\partial^2 T^*}{\partial x_j^* \partial x_j^*} \quad (3)$$

The Rayleigh number is defined by $Ra = (g\beta\Delta TL^3)/(v\alpha)$ and the Prandtl number is $Pr = \nu/\alpha$.

The six walls of the cavity are assumed to be rigid ($u_i = 0$) and at rest. The thermal boundary conditions are $(\partial T^*/\partial n = 0)$ at the four adiabatic lateral walls, and $T_C^* = -0.5$ and $T_H^* = 0.5$ at the top and bottom plates, respectively.

Dissipation has not been included in the energy equation (3) because calculations carried out including this term showed that it is on average five orders of magnitude

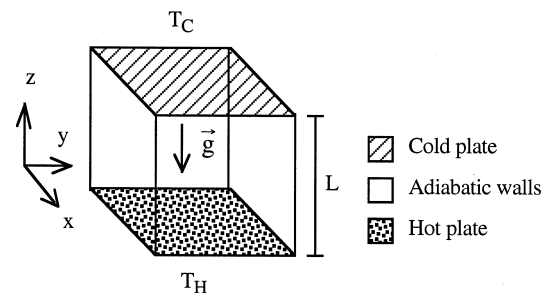


Fig. 1. Physical model.

smaller than diffusion at $Pr = 130$ and $Ra = 6 \times 10^4$. The relative importance that dissipation may attain in very localized regions of the flow where diffusion becomes very small is not sufficient to affect significantly the circulatory patterns calculated in the present study.

3. Numerical scheme

The governing equations (1)–(3) were solved numerically with the FORTRAN code 3DINAMICS. This code has been successfully tested by Cuesta [13] and Cuesta et al. [14] in a lid-driven cavity problem and also in an enclosure with natural convection due to lateral heat transfer [15]. 3DINAMICS uses a finite volume formulation with a second order approximation for the variation of all primitive variables with respect to time and space. A centred scheme is applied for all diffusive terms and a QUICK scheme for the convective fluxes. The code offers the option of an ADI or explicit method for time integration with second order accuracy. The coupling of velocities and pressure is solved following the predictor-corrector scheme SMAC and the Poisson equation for the pressure with a conjugate gradient algorithm. More details about the code are given elsewhere [13, 14].

The fluid was assumed to be initially at rest with a conductive temperature distribution over the domain. In order to start the Rayleigh–Bénard convective regime, a random disturbance of ± 0.05 in the temperature field was added to this initial thermal field. This procedure avoids the predetermination of the final convective structure. Finally, the flow and thermal fields obtained for each convective structure at a given Rayleigh and Prandtl number were successively used as initial conditions for other numerical calculations.

Calculations covered the entire cubical cavity, i.e., no symmetry conditions were adopted, because flow transitions between different structures are asymmetrical and unsteady in nature. Table 1 summarizes the grid independence study carried out for the flow structure yielding the highest heat transfer rates at $Pr = 0.71$ and $Pr = 130$ with uniform grids of 31^3 , 41^3 , 51^3 and 61^3 nodes. A uniform grid distribution was selected to minimize the effects of numerical viscosity and to enforce second-order accuracy. Furthermore, the different roll structures that develop generate regions of high velocity and temperature gradients away from the walls, and the location of these regions are not known *a priori*.

Table 1 shows how the average Nusselt ($Nu_s = h_s L/k$), the maximum local Nusselt number (Nu_l) and its location at the bottom plate change with grid refinement. Since no significant change for both averaged and local quantities is observed in the table for grids with 41^3 or more nodes, this grid was adopted in the present study. According to the experimental thickness of the thermal boundary layer for turbulent natural convection reported by

Table 1
Effect of the grid density on the surface averaged Nusselt number

	Grid			
	31^3	41^3	51^3	61^3
<i>Pr</i> = 0.71				
Nu_s	3.67	3.68	3.68	3.68
Max (Nu_l)	6.16	6.15	6.14	6.14
<i>x</i> Max (Nu_l)	0.22	0.23	0.23	0.23
<i>y</i> Max (Nu_l)	0.74	0.73	0.73	0.73
<i>Pr</i> = 130				
Nu_s	3.80	3.76	3.75	3.75
Max (Nu_l)	6.23	6.14	6.10	6.08
<i>x</i> Max (Nu_l)	0.26	0.25	0.25	0.25
<i>y</i> Max (Nu_l)	0.74	0.75	0.75	0.75

Maximum value of the local Nusselt number and its position in the hot plate at $Ra = 6 \times 10^4$ for the four roll structure with each rotation axis perpendicular to one lateral wall.

Belmonte et al. [16], $\delta = 1/(2 Nu)$, at least four nodes are located within this boundary layer with the 41^3 uniform grid over the range of conditions studied. This grid captures the same dynamical features as a uniform 81^3 grid for the S4 to S1 transition at $Pr = 130$ and, therefore, it was also considered sufficient to describe time dependent phenomena.

The code has been also validated for time dependent convection in cavities of aspect ratios $L_x/L_z = 3.5$ and $L_y/L_z = 2.1$ at $Pr = 2.5$ by comparing present predictions with the experimental results of Gollub and Benson [17] and the numerical results of Mukutmoni and Yang [18]. Gollub and Benson determined that the onset of the time dependent flow occurs at $Ra = 2.9 \times 10^4 \pm 0.2 \times 10^4$. The maximum differences between the velocity fields predicted by Mukutmoni and Yang [18] with the grid $80 \times 80 \times 80$ and by 3DINAMICS with $31 \times 41 \times 51$ nodes is 4% for steady conditions ($Ra = 2 \times 10^4$). The present code predicts the onset of unsteadiness to occur at $Ra = 3 \times 10^4$, in agreement with the above mentioned experimental and numerical results.

4. Results and discussion

This section is divided into five subsections. First, all the convective structures and bifurcation maps for flow transitions are presented. Secondly, the topological features of the seven different flow structures that develop inside the cubical cavity at $Pr = 0.71$ are presented together with the transitions that occur among them as the Rayleigh number increases. Thirdly, the effects of changing Prandtl number are discussed. Then the results

obtained by increasing or decreasing aspect ratios or tilting the cavity are examined. Finally, the average heat transfer rates at the top or bottom plates are presented for all structures over the complete range of Rayleigh and Prandtl numbers covered in this study.

The second invariant of the velocity gradient tensor, defined by $\Pi = S_{ij} S_{ji} + \Omega_{ij} \Omega_{ji}$, where S_{ij} is the strain tensor and Ω_{ij} the rotation tensor, is used to visualize the topology and circulation patterns caused by any structure present at $Ra \leq 4 \times 10^4$. It should be noted that negative values of Π occur in vortical regions where rotation dominates over strain. However, it has been found that pressure is more appropriate than the second invariant of the velocity gradient tensor to describe the vortical structures at $Ra > 4 \times 10^4$. In this case, regions with moderately low pressure correspond to the roll core and to separation zones where the fluid moves away from both horizontal plates, while the regions with high pressure identify impingement zones at the walls.

4.1. Convective structures and bifurcation map

Seven stable steady flow structures have been obtained numerically in the range $3.5 \times 10^3 \leq Ra \leq 6 \times 10^4$ and for $Pr = 0.71, 10$ and 130 . Table 2 summarizes for each structure the type of topology, the local distribution of Nusselt number at the bottom hot plate and the corresponding surfaces of the vertical velocity component at the horizontal midplane. The locations of maximum values of the local Nusselt number, marked with a plus sign, indicate impingement regions caused by the flow coming from the opposite horizontal plate while minimum values indicate regions of boundary layer development. The topologies of all structures, flow transitions between them and the corresponding heat transfer characteristics are discussed in the following subsections.

Figure 2 depicts the variation of the dimensionless heat transfer coefficient with Rayleigh number at $Pr = 0.71$ for the seven structures given in Table 2. Transition from the conductive state ($Nu = 1$) is observed in this figure at $Ra_c = 3500$ for the single roll structures S1, S2 and S3. Two other unstable critical transitions from the conductive state are obtained by extrapolation of the heat transfer data at $Nu = 1$ in Fig. 2 for the four roll structures S5 ($Ra_c = 6000$) and for the toroidal structure S4 ($Ra_c = 7800$). These transitions and the corresponding structures are unstable because they occur at Rayleigh numbers where the conductive state is unstable.

There are several flow transitions between all structures when the Rayleigh number is increased beyond the above mentioned critical values over the range of Prandtl numbers studied here. The transition between S3 and S7 observed in Fig. 2 occurs only at $Pr = 0.71$. Fig. 3a–c summarize, respectively, the bifurcation map for S2, S4 and S5 as a function of Rayleigh and Prandtl numbers. In these figures irreversible and reversible transitions are

identified by one or two arrows, respectively. It should be noted that the concept of reversibility only expresses in this work the recovery of the initial state of the flow after an increase/decrease of the Rayleigh number. Figure 3a depicts the region where the diagonally aligned structure S2, with a critical Rayleigh number of about 3500, evolves irreversibly to the more stable S1 when the Rayleigh number is increased. Structure S4 develops at a higher critical Rayleigh number and is unstable until the Rayleigh number reaches $Ra = 8.0 \times 10^3$ at $Pr = 0.71$, $Ra = 9.8 \times 10^3$ at $Pr = 10$ and $Ra = 9.9 \times 10^3$ at $Pr = 130$, as shown in Fig. 3b. When the Rayleigh number is further increased this structure evolves irreversibly to S1 for $Pr = 10$ and 130 and reversibly to S6 at $Pr = 0.71$. Figure 3c shows the stability region for structure S5. This structure is stable for $Ra \geq 7.6 \times 10^3$ at $Pr = 0.71$, $Ra \geq 9.3 \times 10^3$ at $Pr = 10$ and $Ra \geq 9.5 \times 10^3$ at $Pr = 130$. Figure 3b clearly illustrates the stabilizing effects produced by the viscous terms in the transitions involving S1 when the Prandtl number increases.

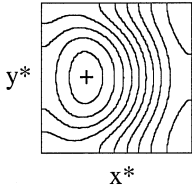
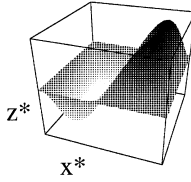
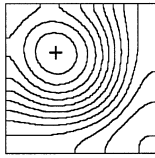
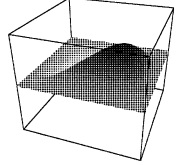
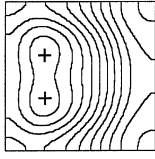
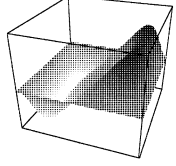
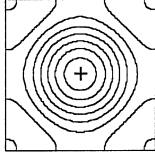
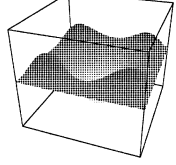
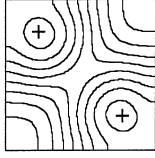
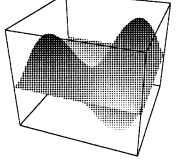
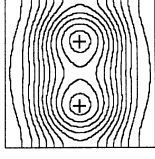
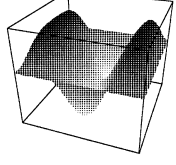
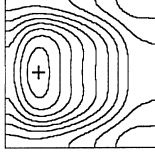
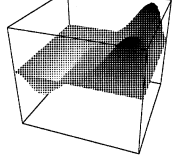
4.2. Structures and transitions at $Pr = 0.71$

The variation of the average Nusselt number with Rayleigh number, given in Fig. 2 for $Pr = 0.71$, indicate that for $Ra \leq 6 \times 10^4$ the seven different structures included in Table 2 may occur inside the cubical cavity. The topologies and the heat transfer characteristics of four of them, S1, S2, S3 and S4, have been already reported in the preliminary work of Pallares et al. [9] for the range $3.5 \times 10^3 \leq Ra \leq 10^4$. Since these structures are the initial or the final step of the flow transitions documented here, they have been also included in Figs 5(b-5, t-5 and f-5), 5(b-1, t-1 and f-1), 7(b-1, t-1 and f-1) and 6(b-1, t-1 and f-1). In addition, a new steady four roll structure S5 has been characterized in the present study. The topology of S5, the corresponding thermal field and distributions of local Nusselt numbers at the two horizontal plates are presented in detail in Fig. 4.

Structure S5 produces four recirculating motions in planes nearly parallel to the four lateral walls, with two ascending currents of hot fluid along two diagonally opposite vertical edges. These currents impinge at the top plate causing two opposing maxima in the heat transfer rate distribution. There, the deflected flow is distributed into two nearly perpendicular currents that reach the two other opposite corners. In these corners the cooling produces descending currents parallel to the other two opposite vertical edges, yielding the corresponding maxima of heat transfer rates at the bottom plate. This mode of circulation can be represented as a four roll structure with axis of rotation centred at each vertical wall. The particle paths shown also in Fig. 4 clearly depict the circulation around two of the four rolls of structure S5.

The increase of the Rayleigh number from $Ra = 10^4$ to 1.5×10^4 at $Pr = 0.71$ affects differently the stability of

Table 2
Convection structures developed in a cubical cavity

Structure	Flow description	<i>Nu</i> distribution	Vertical velocity
S1	Single roll		
S2	Single diagonally oriented roll		
S3	Single roll elongated towards two opposite horizontal edges		
S4	Nearly toroidal roll		
S5	Four roll structure. Each one with its axis perpendicular to one sidewall		
S6	Two parallel roll structure		
S7	Structure S3 with merged descending currents		

The range is $3.5 \times 10^3 < Ra < 6 \times 10^4$ and $Pr = 0.71, 10$ and 130

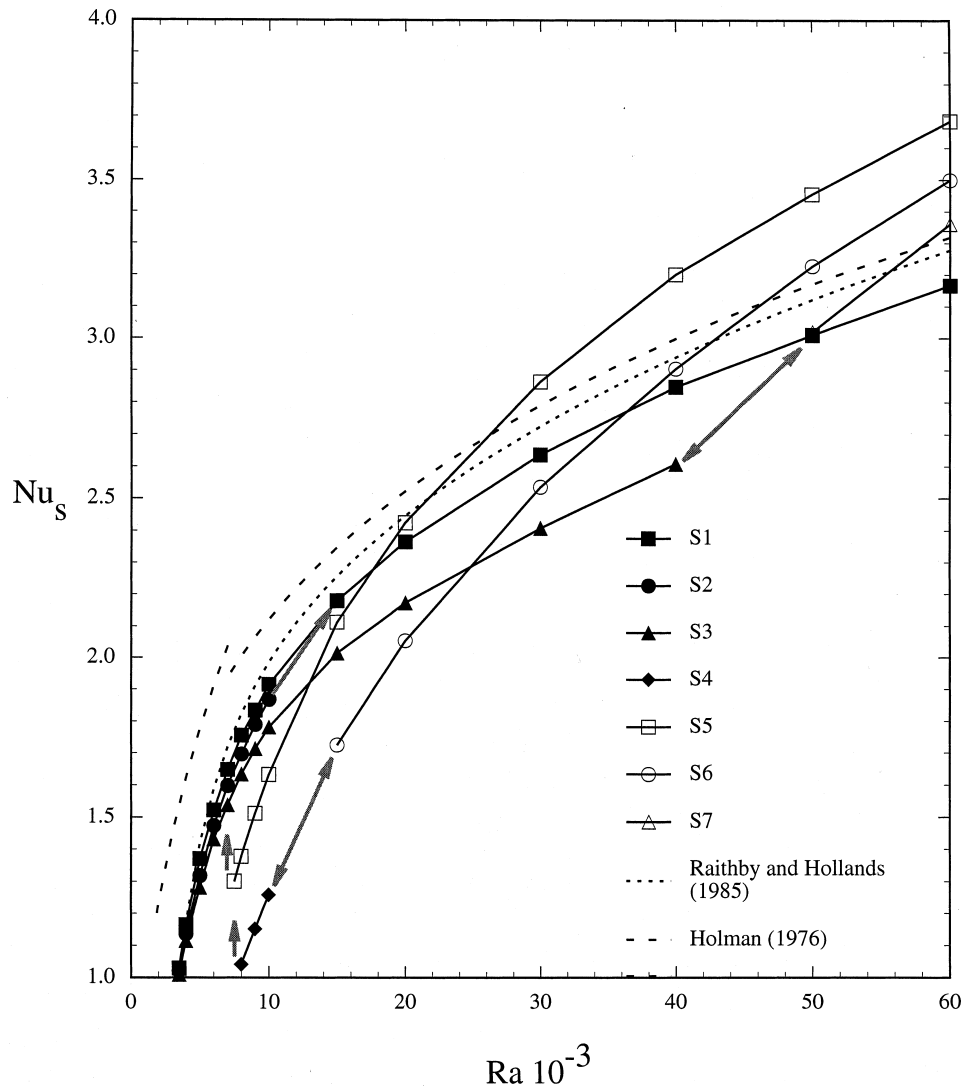


Fig. 2. Average Nusselt number evolutions at $Pr = 0.71$ for all convective structures identified.

the five structures S1–S5 described above. Two discrete flow transitions occur for structures S2 and S4, as shown in Fig. 2. This increase in Rayleigh number produces the evolution of the diagonal aligned roll of S2 to the structure S1. This transition is summarized in Fig. 5 for an increase from $Ra = 10^4$ to 2×10^4 , in terms of the evolution of the distribution of local Nusselt numbers, the second invariant Π and surfaces of equal temperature. The increase in the input of energy caused by the change in the Rayleigh number, increases initially the heat transfer rates (Fig. 5.b-2 and t-2), as expected. While the diagonal topology is maintained as time advances, a destabilizing effect produces a slight displacement of the structure across the y direction, with a corresponding loss

of the diagonal symmetry of the roll (Fig. 5.b-3 and t-3). Then, the surface-averaged Nusselt number decreases and the heat transfer rate regions expand along the y direction (Fig. 5.b-4 and t-4), until the final steady state S1 structure is reached (Fig. 5.b-5 and t-5).

It is interesting to note in Fig. 5 that S1 presents at $Ra = 2 \times 10^4$ two maxima of heat transfer rate on each plate instead of the single maximum reported by Pallares et al. [9] at $Ra = 10^4$. As it will become clear in what follows, this is a common feature of the behaviour of single rolls when Ra is increased because the corresponding increase in the rate of fluid circulation forces the structure to adapt itself to the restricted space of the cavity by adopting the form of a double wheel. Present

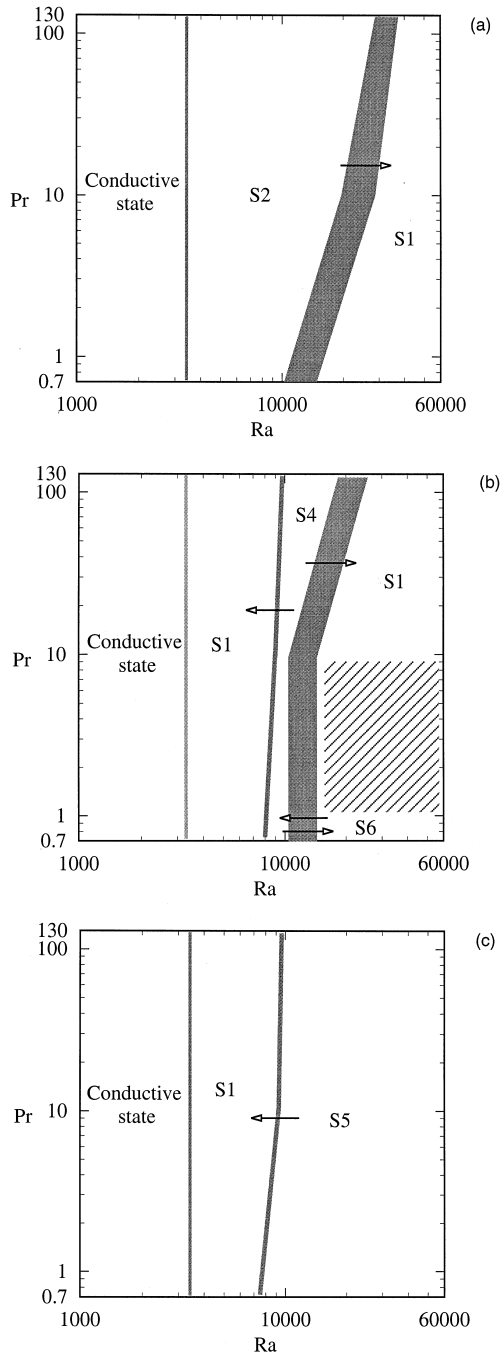


Fig. 3. Bifurcation map for structures (a) S2; (b) S4; (c) S5.

results shown that this transition from S2 to S1 is irreversible, i.e., S2 is not recovered when Ra is decreased from 2×10^4 or 1.5×10^4 to 10^4 . The irreversible nature of this transition does not mean that S2 is intrinsically unstable for $Ra \leq 10^4$.

A second flow transition from S4 to S6 is observed in Fig. 2 when the Rayleigh number is increased from $Ra = 10^4$ to 1.5×10^4 at $Pr = 0.71$. The evolution of the velocity and temperature fields, as well as of the local Nusselt number in the two horizontal plates is shown in Fig. 6 for a steeper change from $Ra = 10^4$ to 2×10^4 . In this case the imposed increase in energy flux cannot be effected by structure S4 in an evenly spatially distributed manner due to the presence of the lateral walls. It can be seen in Fig. 6 that at the bottom hot plate the central region of high heat transfer rates is enlarged, preserving the diagonal symmetry, while at the top cold plate this symmetry is broken (Fig. 6.b-2 and t-2). This seems to be the first step in the instability mechanism associated with the flow transition S4 to S6. As time advances (Fig. 6.b-3 and t-3; 6.b-4 and t-4) the flow tends towards a new two roll configuration S6 through the opening of the S4 toroidal roll.

The flow topology of the new S6 structure shown in Fig. 6.f-5, in terms of the second invariant Π , and in Table 2 reveals two centres of rotation with their axis parallel to two opposite sidewalls. The thermal field indicates the existence of two main ascending motions parallel to two opposite sidewalls, which are deflected towards the centre of the top plate. The cooling of the fluid in these two opposite motions in the upper region produces a descending current in the central vertical plane of the cavity which impinges at the lower plate, yielding two separate impingement regions, as shown in Fig. 6.b-5. The maps of local Nusselt indicate that the two rolls of structure S6 not only rotate around the x -axis but also around the y -axis. This is the reason why there are two maxima at the bottom plate and only two (and not four, as could be expected) at the top plate. This behaviour can be understood as the result of a contribution of two x -rolls and two y -rolls, according to the terminology of Catton [3] but with the x -rolls being dominant over the y -rolls. Thus, the topology of S4 and S6 have a common basis, despite the fact that their appearance is different. In this case the flow transition is reversible, i.e., when Ra is decreased again to 10^4 the structure S6 evolves exactly to S4.

Figure 2 shows that when the Rayleigh number is increased beyond 4×10^4 at $Pr = 0.71$ structure S3 evolves into a rather similar structure named S7. The topology of S3 at $Ra = 4 \times 10^4$ is shown in Table 2 and Fig. 7 in terms of isosurfaces of pressure. As it happens with S1, the increase in Ra produces an intensification of the circulation at the two sides of the structures, giving rise to a form similar to a double wheel. While the two wheels of the structure remain parallel when Ra increases in the case of S1, they progressively and laterally separate at one side of the cavity and get closer at the other in S3.

The effect of the impinging currents associated to these two zones of stronger circulation are clearly shown in the local Nusselt numbers distributions plotted in Fig. 7.

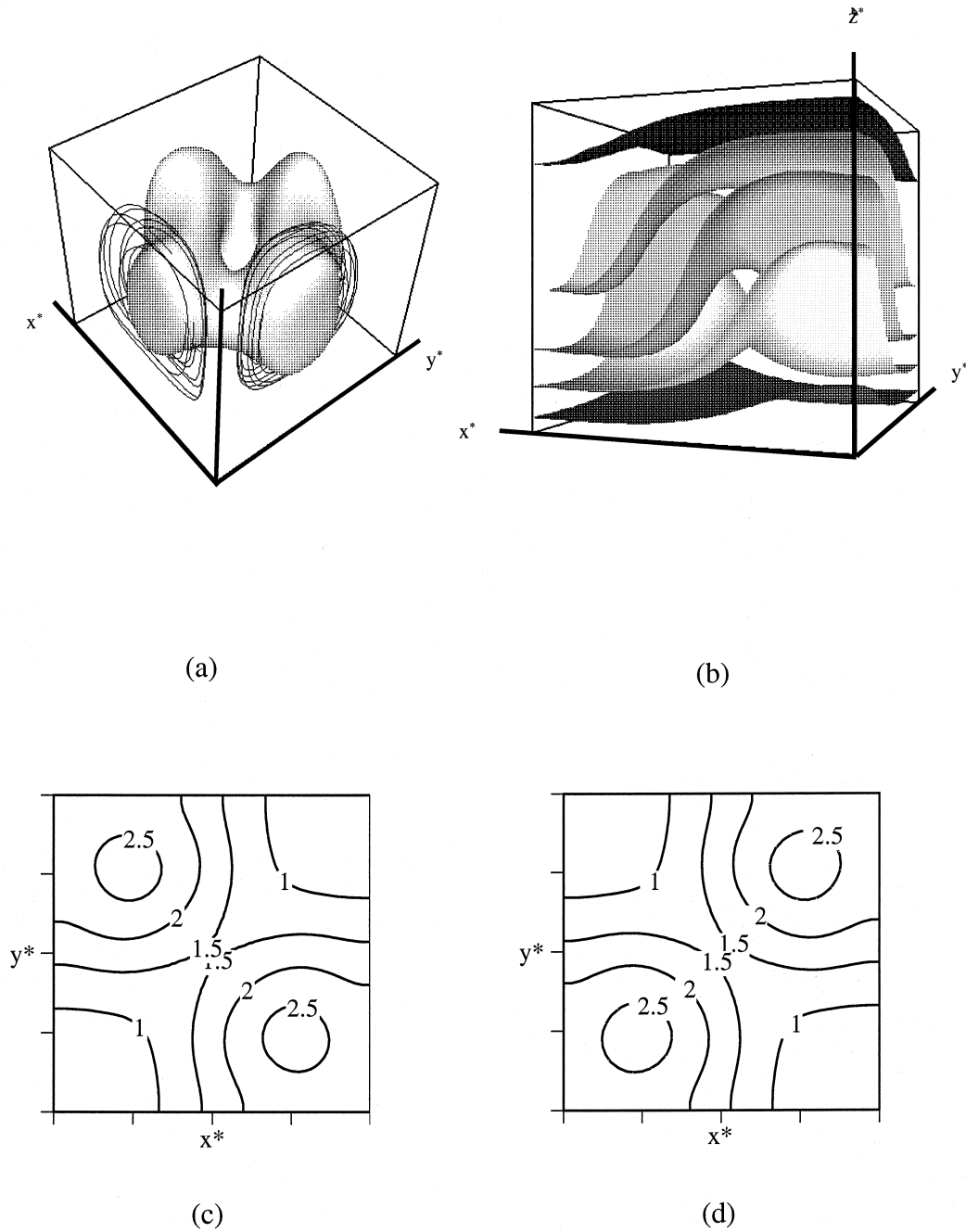


Fig. 4. Structure S5 at $Ra = 10^4$. (a) Dynamical field, $\Pi^* = -2000$. (b) Thermal field, isosurfaces of temperature $T^* = 0.4, 0.2, 0.0, -0.2$ and -0.4 . (c) Nusselt number distribution in the bottom hot plate. (d) Nusselt number distribution in the top cold plate.

When the Ra increases from 4×10^4 to 5×10^4 the two circulating zones in S3 become stronger and definitively merge at the central plane of symmetry of the cavity, yielding S7. Therefore, instead of the two zones of maximum heat transfer rates at the bottom wall present

in structure S3, a single and completely symmetrical zone of high transfer rates occurs in structure S7. Both structures yield two zones of maximum heat transfer at the top plate.

Taking into account the three flow transitions

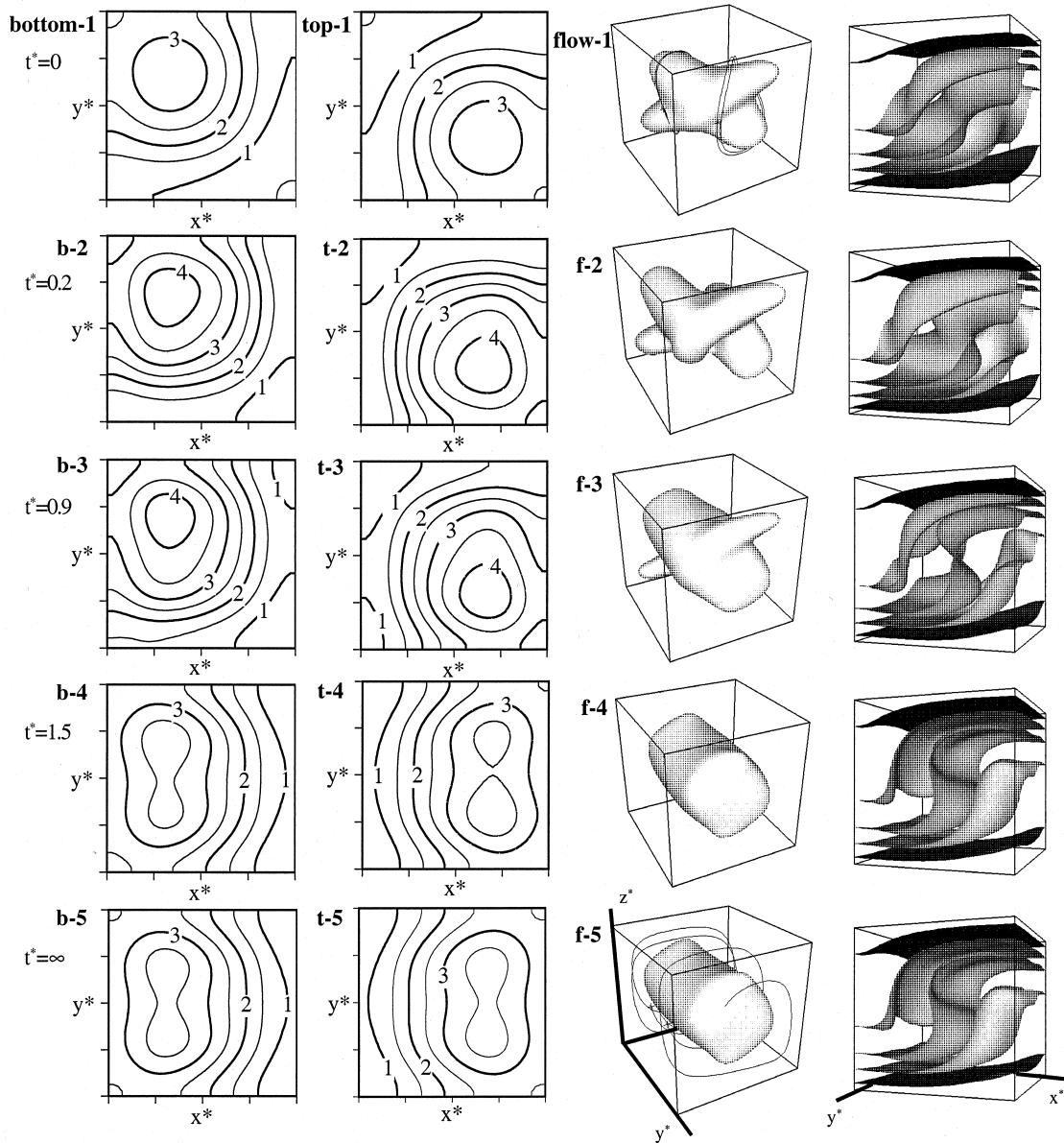


Fig. 5. Time evolution for the irreversible flow transition at $Pr = 0.71$ from structure S2 at $Ra = 10^4$ (b-1, t-1 and f-1) to structure S1 at $Ra = 2 \times 10^4$ (b-5, t-5 and f-5). (bottom-1 to b-5 and top-1 to t-5) Nusselt number distributions in the bottom cold plate and in the top cold plate. (flow-1 to f-5) Dynamical and thermal fields: (flow-1) $\Pi^* = -3000$; (f-2) $\Pi^* = -3000$; (f-3) $\Pi^* = -3000$; (f-4) $\Pi^* = -3000$; (f-5) $\Pi^* = -3000$.

described above, only convective structures S1, S5, S6 and S7 exist at $Ra = 5 \times 10^4$ and remain stable at least up to $Ra = 6 \times 10^4$ for $Pr = 0.71$. The effect of increasing the Rayleigh number on these structures may be summarized as follows. Structure S1 has a single roll shape (see Table 2 and Fig. 5.f-5) for $Ra > 10^4$, with strong circulation at the extremes. This is also the case in structure S3 up to $Ra = 4 \times 10^4$ and structure S7 for higher Ra . Both the

absolute maximum value of local Nusselt numbers and the separation between the two maxima at the bottom and top plates increased with Ra in these structures.

On the other hand, the flow rate of the two circulations present in S3 increase in structure S7 due to the progressive displacement of the extremes of the roll towards the top plate (Fig. 7.f) when the Rayleigh number is increased. This feature has also been observed by Kos-

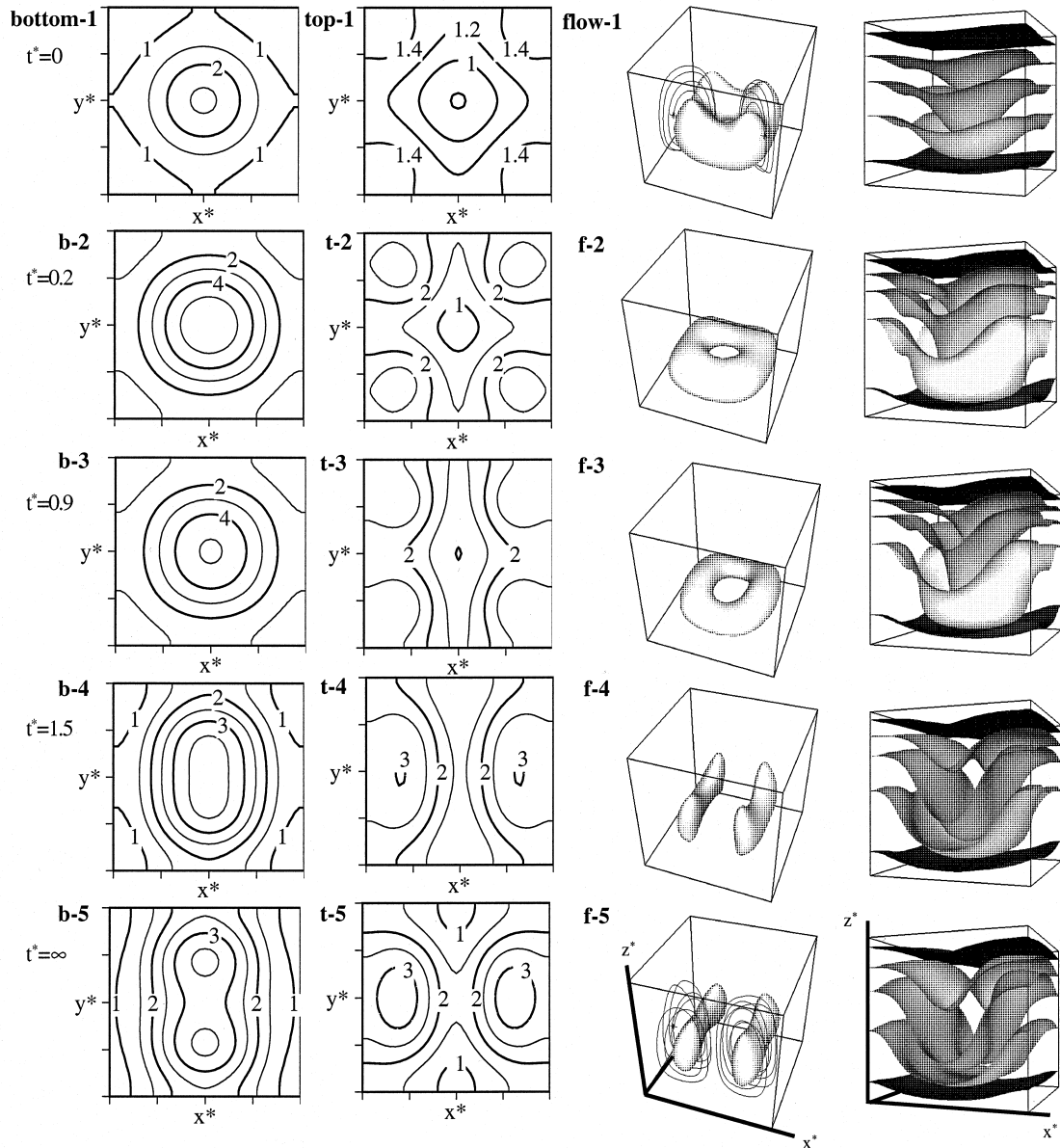


Fig. 6. Time evolution for the reversible flow transition at $Pr = 0.71$ from structure S4 at $Ra = 10^4$ (b-1, t-1 and f-1) to structure S6 at $Ra = 2 \times 10^4$ (b-5, t-5 and f-5). (bottom-1 to b-5 and top-1 to t-5) Nusselt number distributions in the bottom cold plate and in the top cold plate. (flow-1 to f-5) Dynamical and thermal fields: (flow-1) $\Pi^* = -1000$; (f-2) $\Pi^* = -10000$; (f-3) $\Pi^* = -14000$; (f-4) $\Pi^* = -15000$; (f-5) $\Pi^* = -13000$.

chmieder [19] and Yang [8] in large aspect ratio enclosures where the rolls that develop increase their wavelength to provide extra space for circulation when the Rayleigh number increases. This phenomenon may be attributed to three-dimensional instabilities when it is associated with a discrete loss of rolls [20]. In the cubical cavity, the process is dominated by the lateral walls because the number of rolls cannot be reduced.

Structure S6, shown in Table 2 and Fig. 6.f-5, maintains its main dynamic and thermal characteristics in the range of Rayleigh numbers from 10^4 to 6×10^4 . When the Rayleigh number increases circulation increases and the impingement zones at the top and bottom plates (Fig. 6.b-5 and t-5) broaden and the corresponding values of the local Nusselt number increase. Structure S5 also retains the same topological characteristics over the range

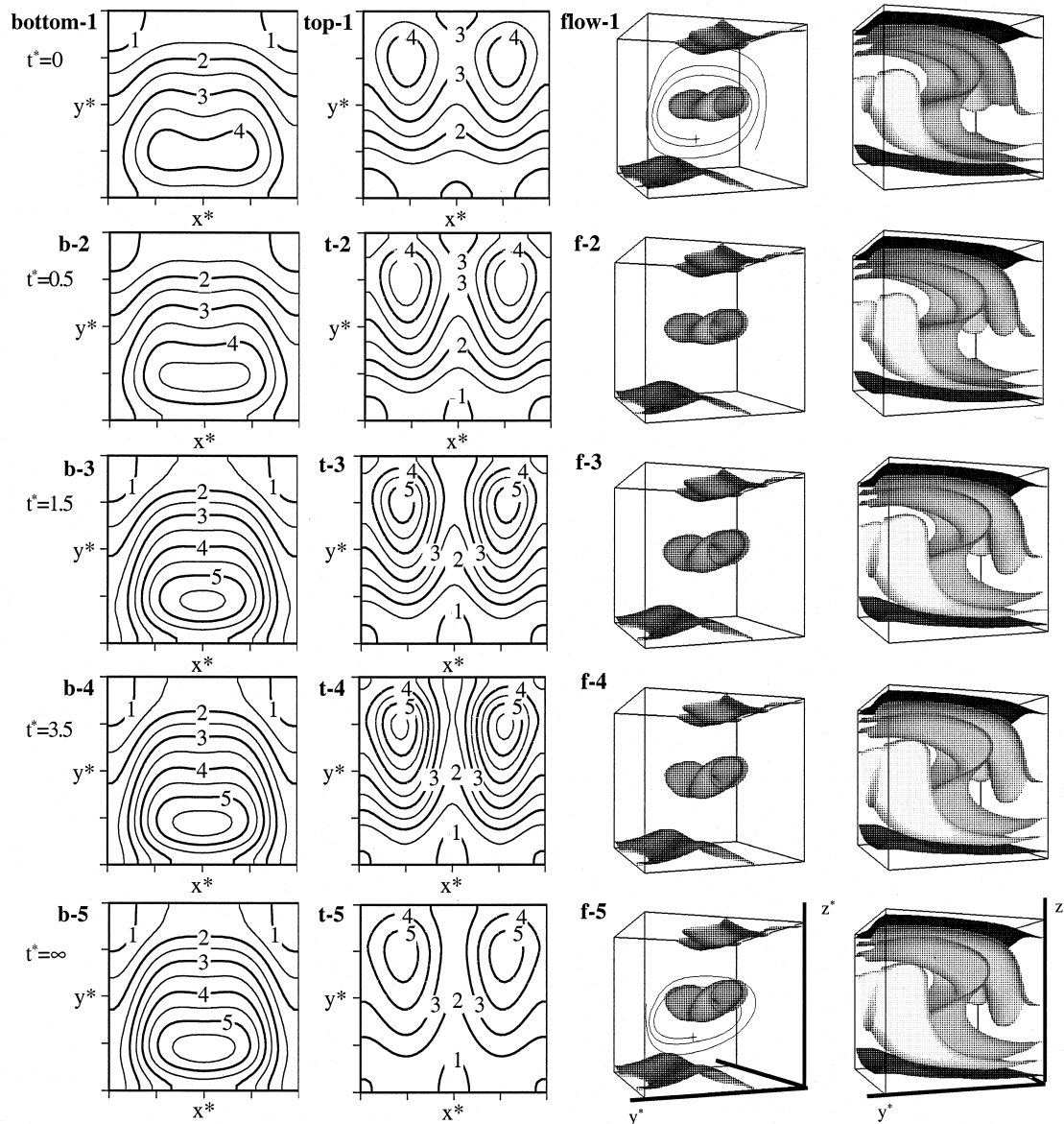


Fig. 7. Time evolution for the reversible flow transition at $Pr = 0.71$ from structure S3 at $Ra = 4 \times 10^4$ (b-1, t-1 and f-1) to structure S7 at $Ra = 5 \times 10^4$ (b-5, t-5 and f-5). (bottom-1 to b-5 and top-1 to t-5) Nusselt number distributions in the bottom cold plate and in the top cold plate. (flow-1 to f-5) Pressure and thermal fields: (flow-1) $P^* = -1000$; (f-2) $P^* = -1200$; (f-3) $P^* = -1200$; (f-4) $P^* = -1200$; (f-5) $P^* = -1200$.

of conditions studied, with a more intense circulation and higher transfer rates at the two horizontal at higher Rayleigh numbers.

4.3. Prandtl number effect on flow transitions

The effects of increasing the Prandtl number or the relative importance of viscosity on the flow inside the

cavity has been studied at $Pr = 10$ and 130 . The increase in Prandtl number from 0.71 up to 130 does not affect the occurrence of structures S1, S2, S4 and S5, but shifts the transitions between them to higher Ra . For example, the irreversible transition from S2 to S1 (see Fig. 3a) that occurs between $Ra = 10^4$ and 1.5×10^4 at $Pr = 0.71$, takes place between $Ra = 2 \times 10^4$ and 3×10^4 at $Pr = 10$, and between $Ra = 3 \times 10^4$ and 4×10^4 at $Pr = 130$, due to the

increasing relative influence of viscosity on the cavity flow. This tendency is even more prominent for the new transition found between S4 and S1 when $Pr > 0.71$, as shown in Fig. 3b. The small effect of Prandtl number on the irreversible transition from S5 to S1 near the unstable critical transition from the conductive state ($Ra_c = 6000$ in Fig. 2) is illustrated in Fig. 3c.

An increase in Prandtl number also affects the stability of structures S3 and S7, as well as the transition from S4 to S6 (see Fig. 3b). The single and elongated roll structures S3 and S7 cannot be stabilized for $Pr \geq 10$ when the S3 structure obtained at $Pr = 0.71$ is used as initial condition. However, it is possible to obtain structures S6 at $Ra = 5 \times 10^4$ and S7 at $Ra = 6 \times 10^4$ and $Pr = 10$ and 130 using these structures at $Pr = 0.71$ as initial conditions. Structure S6 evolves to S5 and structure S7 to S1 when the Rayleigh number is decreased from 5×10^4 to 4×10^4 and from 6×10^4 to 5×10^4 , respectively. On the other hand, the transition from S4 to S6, established in Fig. 3b and illustrated in Fig. 6 for $Pr = 0.71$, is substituted by a new irreversible transition between S4 and S1 at $Pr = 10$ and 130. Figure 8 depicts the sequences in the evolution of the local Nusselt number distributions at the horizontal plates and the thermal and dynamic fields pertaining initially to S4 when the Rayleigh number is increased from 3×10^4 to 4×10^4 at $Pr = 130$. While for the transition from S4 to S6 at $Pr = 0.71$ there is a conservation of the two symmetry planes perpendicular to the four sidewalls (see Fig. 6), the transition from S4 to S1 breaks all the symmetry planes through a complex flow redistribution as revealed by the evolution of the local Nusselt number fields given in Fig. 8.

4.4. Aspect ratio and tilting effects on structure stability

The circulation and/or orientation of the seven structures included in Table 2 could be sensitive to small changes in the cubical geometry. Table 3 illustrates the response of the four possible structures S1, S2, S4 and S5 at $Ra = 10^4$ and $Pr = 130$ to three destabilizing effects: (i) An increase of 10% in the horizontal x -direction ($1.1 \times 1 \times 1$), (ii) an increase or (iii) decrease up to 20% in both horizontal x - and y -directions ($1.1 \times 1.1 \times 1$; $1.2 \times 1.2 \times 1$) or ($0.9 \times 0.9 \times 1$; $0.8 \times 0.8 \times 1$). The flow conditions at $Ra = 10^4$ and $Pr = 130$ have been selected because they can be reproduced experimentally with small cavities ($L \leq 0.01$ m) filled with silicon oil.

The results included in Table 3 show that a perturbation of 10% in the horizontal x -direction does not affect the single roll S1_y with vorticity in the y -direction, as expected. This perturbation, however, is sufficient to break the diagonal alignment of S2 and to set in a S1 structure with rotation parallel to two opposing lateral walls. Structure S1 is capable of circulating more fluid than S2 when the two side walls with x -orientation are

separated from each other. The elongation imposed by the perturbation is also sufficient to split the nearly toroidal roll S4 into the two parallel roll structure S6. However, the dominant effect that the four lateral walls have on the four circulatory motions present in S5 is sufficient to maintain the four roll characteristics for a 10% elongation of the x - (or y -) dimension of the cubical cavity.

A 10 and 20% increase in the two horizontal dimensions of the cavity, attained without changing the Rayleigh number, implies a relative decrease in the influence of the lateral walls in structures S1, S2, S4 and S5 at $Ra = 10^4$ and $Pr = 130$. Table 3 shows that all four structures are unaffected by a 10% increase. This is also the case in structures S1, S4 and S5 for the 20% increase. However, structure S2 cannot handle the increase in circulation imposed by the ($1.2 \times 1.2 \times 1$) configuration at $Ra = 10^4$ and evolves to the more efficient circulating pattern of S1. The upward or downward flow rate across the mid-plane in S1 doubles with the 20% increase in dimension. The circulatory motions of structures S4 and S5 remain stable with a rate of circulation three times higher than that for the cubical cavity.

The horizontal reduction in the two horizontal dimensions of the cavity by 10 and 20%, also without changing the vertical dimension or the Rayleigh number, implies a relative increase in the influence of the lateral walls in the structures S1, S2, S4 and S5 present at $Pr = 130$, i.e. under conditions where viscosity plays a significant role. Table 3 indicates that structures S1 and S2 are not sensitive to the reduction in circulation imposed by the larger influence of the lateral walls at $Ra = 10^4$. It should be noted that the upward or downward flow rate across the horizontal mid-plane in structures S1 and S2 is reduced approximately by a factor of three when the lateral dimensions are reduced by 20%. Structures S4 and S5, which involve important interactions between the viscous flow and the four lateral walls, are not so efficient to transport energy under the imposed reduced dimensions and evolve to the single roll S1.

It is also convenient to determine the effect of small vertical misalignments on flow structures, as suggested by Moffat [21]. Tables 4 and 5 illustrate that a slight tilt on the cavity has a stronger effect on the flow than changing the geometry. Table 4 indicates that at $Ra = 10^4$ and $Pr = 130$ even small rotations of $\gamma = 0.1, 0.5$ and 1° around the x -coordinate are sufficient to change the type of flow structure mainly because of the new contribution of the buoyancy term ($Ra Pr T^* \sin \theta$) in momentum equation (2) along the y -direction. As a result, the circulation of structure S1_y is maintained for $\gamma \leq 0.1^\circ$ and it changes to a diagonal orientation typical of S2 at $\gamma = 0.5^\circ$, as an intermediate stage before S1_x is recovered with x -vorticity for $\gamma = 1^\circ$. A tilt of 1° in S1_y is sufficient to cause a rotation of the roll around the z -coordinate and to evolve to S1_x. Correspondingly, structure S2 is

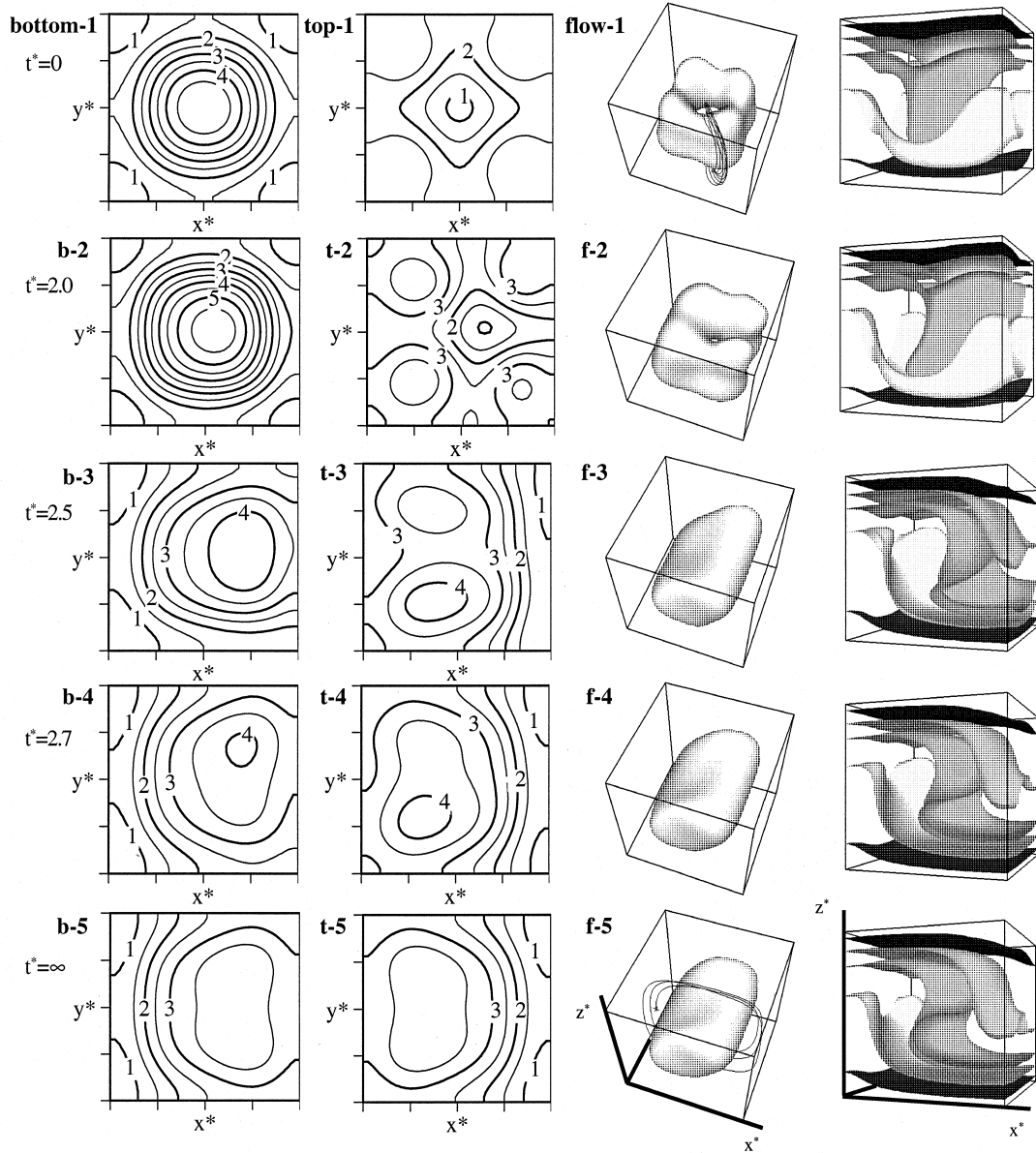


Fig. 8. Time evolution for the irreversible flow transition at $Pr = 130$ from structure S4 at $Ra = 3 \times 10^4$ (b-1, t-1 and f-1) to structure S1 at $Ra = 4 \times 10^4$ (b-5, t-5 and f-5). (bottom-1 to b-5 and top-1 to t-5) Nusselt number distributions in the bottom cold plate and in the top cold plate. (flow-1 to f-5) Dynamical and thermal fields: (flow-1) $\Pi^* = -10000$; (f-2) $\Pi^* = -10000$; (f-3) $\Pi^* = -10000$; (f-4) $\Pi^* = -10000$; (f-5) $\Pi^* = -10000$.

stable for $\gamma \leq 0.5^\circ$ and changes to $S1_x$ at $\gamma = 1^\circ$. At $Ra = 10^4$ and $Pr = 130$ both S4 and S5 are very sensitive to the vertical alignment of the cavity and even at $\gamma = 0.1^\circ$ evolve to $S1_x$.

Table 5 illustrates that the effect of tilting the cavity is less important for the same Prandtl number as the Rayleigh number increases, as expected. At $Ra = 5 \times 10^4$ and $Pr = 130$ both $S1_x$ and S5 are stable for $\gamma = 0.5^\circ$ while

S6 evolves to S1. Therefore, only S1 and S5 are expected to occur in laboratory experiments with small cavities at this Rayleigh number. When the Prandtl number decreases so does the importance of the additional source buoyancy term in the y -momentum equation (2). In the case of $Pr = 0.71$, structures $S1_y$, S7, S5 remain stable up to $\gamma = 0.5^\circ$ at $Ra = 5 \times 10^4$, while S6 evolves to S7, as indicated in Table 5.

Table 3
Influence of small changes in the aspect ratio on the stability of structures present in a cubical cavity

Initial structure $Ra = 10^4; Pr = 130$	Destabilizing effect				
	$1.1 \times 1 \times 1$	$1.1 \times 1.1 \times 1$	$1.2 \times 1.2 \times 1$	$0.9 \times 0.9 \times 1$	$0.8 \times 0.8 \times 1$
S1 _y	S1 _y	S1	S1	S1	S1
S2	S1 _y	S2	S1	S2	S2
S4	S6	S4	S4	S1	S1
S5	S5	S5	S5	S5	S1

$Ra = 10^4$ and $Pr = 130$.

Table 4
Influence of a tilt of $\gamma = 0.1^\circ, 0.5^\circ$ and 1° around the x -coordinate on the stability of the structures

Initial structure $Ra = 10^4; Pr = 130$	Destabilizing effect		
	$\gamma = 0.1^\circ$	$\gamma = 0.5^\circ$	$\gamma = 1^\circ$
S1 _y	S1 _y	S2	S1 _x
S2	S2	S2	S1 _x
S4	S1 _x	S1 _x	S1 _x
S5	S1 _x	S1 _x	S1 _x

$Ra = 10^4$ and $Pr = 130$.

Table 5
Influence of a tilt of $\gamma = 0.5^\circ$ around the x -coordinate on the stability of the structures

Initial structure $Ra = 5 \times 10^4$	Destabilizing effect	
	$\gamma = 0.5^\circ; Pr = 0.71$	$\gamma = 0.5^\circ; Pr = 130$
S1 _y	S1 _y	S1 _y
S7	S7	—
S5	S5	S5
S6	S7	S1

$Ra = 5 \times 10^4$ and $Pr = 0.71$ and 130 .

4.5. Average heat transfer rates

The multiplicity of flow structures present in the Rayleigh–Bénard convection in a cubical enclosure produces different Nusselt numbers at the two horizontal plates, as indicated in Table 2 and in Figs 4–8. Figure 2 shows the evolution of the surface-averaged Nusselt number for the seven convective structures present for $Ra \leq 6 \times 10^4$

at $Pr = 0.71$. Figure 9 summarises the variation of the average Nusselt numbers with Rayleigh number for the structures that are stable at the three Prandtl numbers studied, i.e., structures S1 (Fig. 9a), S2 (Fig. 9b), S4 (Fig. 9c) and S5 (Fig. 9d). The last three figures include also the heat transfer characteristics of S1 as a reference. The transitions discussed in subsections 4.1, 4.2 and 4.3 are marked in Figs 2 and 9 with arrows.

The results plotted in Fig. 9 indicate that the average heat transfer rates increase by about 3% when the Prandtl number is increased from $Pr = 0.71$ to $Pr = 10$ in supercritical conditions. Beyond $Pr = 10$, no significant increase is observed for any convective structure because of the limiting effect that the sidewalls have on the flow when the effect of viscosity is important. Structures S1 (Fig. 9a), S2 (Fig. 9b) and S3 (Fig. 2) yield similar heat transfer rates at low Rayleigh numbers, while they are smaller for the four roll structure S5 (Fig. 9d) and even more so for the toroidal S4 (Fig. 9c) or double roll S6 (Figs 2 and 9c). This performance for transferring heat reverses at higher Rayleigh numbers.

The average Nusselt number for the similar single roll structures S1 and S3 follows a similar variation with Rayleigh number, $Nu_s \propto Ra^{1/4}$, for $Ra > 1.5 \times 10^4$, as shown in Figs 2 and 9a. This variation is equivalent to that for an upper surface of a heated plate or the lower surface of a cooled plate. Structure S1 induces, however, higher recirculating upward or downward flow rates across the horizontal midplane than S3 for the same Rayleigh number, and so are the corresponding average transfer rates. When Ra increases beyond 4×10^4 , the corresponding increase in heat transfer rates at the upper and lower plates cannot be accomplished efficiently by the relatively weaker recirculating motion set in by S3 and a new, similar, but more effective structure S7 evolves. This new structure S7 transfers heat more efficiently, with a dependency $Nu_s \propto Ra^{1/2}$, because the heat transfer process is dominated more by an impinging flow rather than by a rolling motion, as discussed previously (see Fig. 7). At $Ra = 6 \times 10^4$ structure S7 yields average transfer rates that are already higher than for S1.

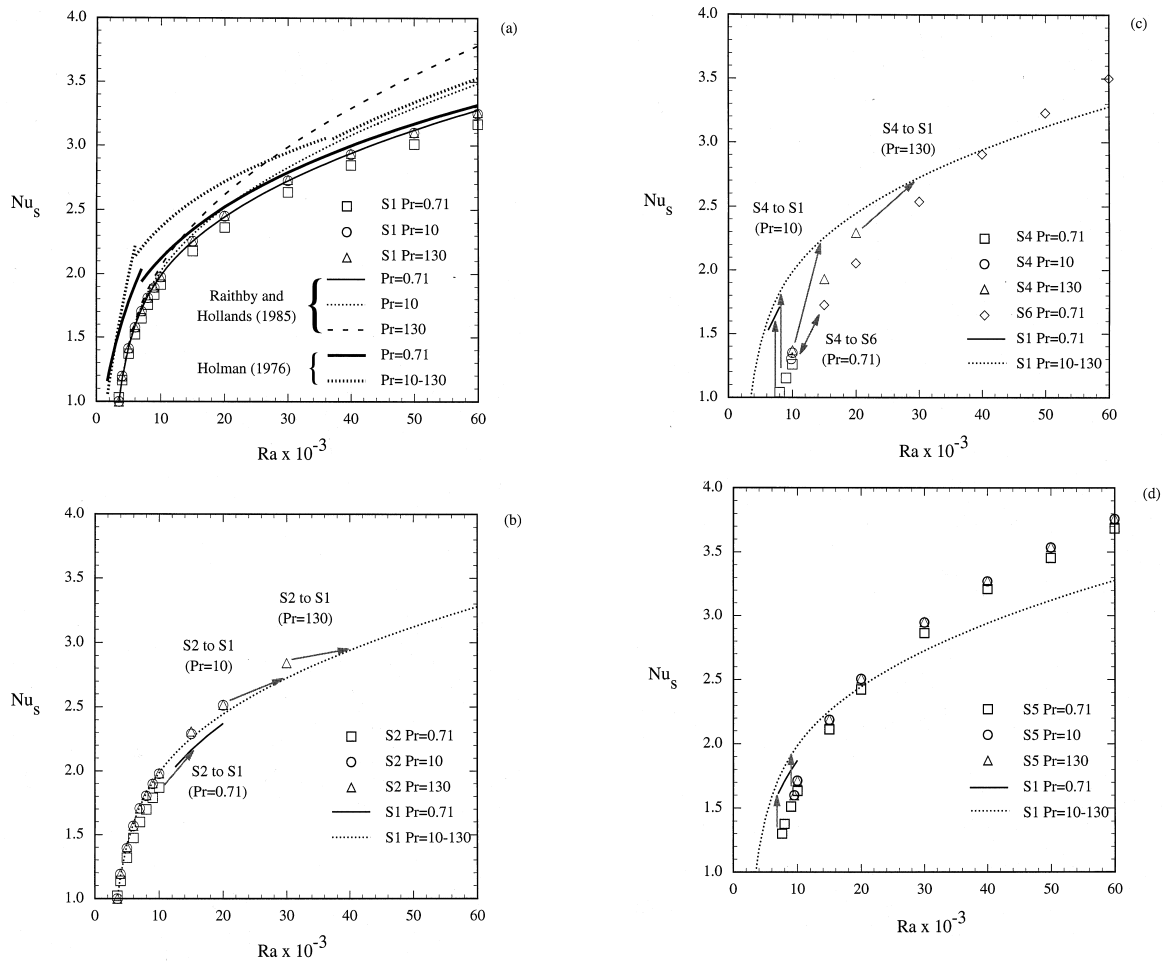


Fig. 9. Variation of the average Nusselt number with Rayleigh number at $Pr = 0.71, 10$ and 130 , for (a) structure S1, (b) structure S2, (c) structure S4 and S6, and (d) structure S5.

On the other hand, the average Nusselt numbers predicted for the four roll S5 and S6 follow a dependency $Nu_s \propto Ra^{1/2}$ similar to that for S7 because, as opposed to S1 and S3, they generate single plumes and impinging jets at both plates, as shown in Figs 4 and 6, respectively. The four roll geometry of S5 is the most efficient transferring energy at high Ra because the jets and plumes that are generated at the corners minimize the effects of the lateral walls on convection.

When the numerically predicted heat transfers rates given in Figs 2 and 9 for all structures are compared globally with the correlations of Raithby and Hollands [22] and Holman [23] a general agreement is found. The different branches of the correlation of Holman [23] correspond to $Ra < 7000$ and $Ra > 7000$ for $Pr = 0.71$, to $Ra < 6000$ and $Ra > 6000$ for $Pr = 10$, and to $Ra < 37000$ and $Ra > 37000$ for $Pr = 130$. Present heat

transfer calculations for S1, S2 and S3 yield lower transfer rates than the correlation of Holman [23] near the critical Rayleigh number. It should be noted that this correlation does not account for the increasing importance of the lateral walls as the Rayleigh number diminishes and, in the limit, predicts a critical Rayleigh number around 1700, which corresponds to Rayleigh–Bénard flow between two infinite horizontal plates. At higher Rayleigh numbers deviations are of the order of 9% and the trend of the variation of the present predictions with Ra and Pr is in agreement with that of the correlation.

Best agreement is found in Figs 2 and 9a with the correlation of Raithby and Hollands [22] because the critical Rayleigh numbers for enclosures was imposed in this case. Numerically predicted average Nusselt numbers for S1 are about 4% lower than those calculated from the correlation at $Pr = 0.71$ over the whole range of Rayleigh

numbers studied. Deviations increase with Rayleigh number for $Pr = 10$ and $Pr = 130$, reaching a maximum value of 13%, because the correlation estimates higher Nusselt numbers in the case of high Prandtl number fluids in enclosures with small aspect ratios.

5. Summary remarks

The detailed numerical study of the natural convection in a cubical enclosure at moderate Rayleigh numbers has revealed the existence of seven different flow structures, with their intrinsic stability depending on the value of the Rayleigh and Prandtl numbers. Several flow transitions have been observed, some of them being irreversible. In the range $10^4 \leq Ra \leq 6 \times 10^4$ only two different structures; the single roll, S1 and the four roll, S5; exist for all possible values of Rayleigh and Prandtl numbers and for vertical misalignments up to 0.5° . This is also the case for the single roll S7 at $Ra = 6 \times 10^4$. The occurrence of other structures is limited to a narrower range of Rayleigh numbers. The destabilizing perturbation caused by a 10% increase or decrease in both horizontal dimensions of the cubical cavity at $Ra = 10^4$ and $Pr = 130$ has little effect on the single roll (S1 and S2) and four roll (S5) structures present at these conditions. The nearly toroidal roll S4 while insensitive to a lateral expansion of the cavity cannot maintain its recirculating pattern when the lateral walls get closer to each other and viscous effects increase, and evolves into a single roll S1.

Predicted transfer rates for single roll structures follow the Nusselt number 0.25 dependency on the Rayleigh number given by correlations reported in the literature for free convection in enclosures. For the highly unstable toroidal and double roll structures and the stable four roll topology the flow that develops at the plates includes impingement regions and this dependency increases up to the 0.5 power of Rayleigh number. There is general agreement between present predictions and available correlations. The analysis of the reported flow transitions and characteristics of the different structures present in the cubical cavity, provide valuable information about flow instabilities and the onset of unsteadiness for free convection in enclosures.

Acknowledgements

The authors would like to acknowledge the financial support received from DGICYT projects PB93-0656-C02-01 and PB96-1011. One of the authors (J.P.) would like to thank the support received from the Cray Research Center in Eagan (MN) to carry out most of the calculations on the Cray supercomputers C-90 and J-90 and to gratefully acknowledge the corresponding financial

support received from the Fundació Catalana per la Recerca.

References

- [1] F.H. Busse, Transition to turbulence in Rayleigh–Bénard convection, in: H.L. Swinney, J.P. Gollub (Eds.), *Hydrodynamic instabilities and the transition to turbulence*, Springer, New York, 1981, pp. 97–137.
- [2] S.H. Davis, Convection in a box: linear theory, *J. Fluid Mechanics* 30 (1967) 465–478.
- [3] I. Catton, The effect of insulating vertical walls on the onset of motion in a fluid heated from below, *Int. J. Heat Mass Transfer* 15 (1972) 665–672.
- [4] W.L. Heitz, J.W. Westwater, Critical Rayleigh numbers for natural convection of water confined in square cells with L/D from 0.5 to 8, *ASME J. Heat Transfer* 93 (1971) 188–196.
- [5] K. Stork, U. Müller, Convection in boxes: experiments, *J. Fluid Mechanics* 54 (1972) 599–611.
- [6] R. Kessler, Nonlinear transition in three-dimensional convection, *J. Fluid Mechanics* 174 (1987) 357–379.
- [7] K.R. Kirchartz, H. Oertel, Three-dimensional thermal cellular convection in rectangular boxes, *J. Fluid Mechanics* 192 (1988) 249–286.
- [8] K.T. Yang, Transitions and bifurcations in laminar buoyant flows in confined enclosures, *ASME J. Heat Transfer* 110 (1988) 1191–1203.
- [9] J. Pallares, I. Cuesta, F.X. Grau, F. Giralt, Natural convection in a cubical cavity heated from below at low Rayleigh numbers, *Int. J. Heat Mass Transfer* 39 (1996) 3233–3247.
- [10] H. Ozoe, K. Yamamoto, S.W. Churchill, H. Sayama, Three-dimensional, numerical analysis of laminar natural convection in a confined fluid heated from below, *ASME J. Heat Transfer* 98 (1976) 202–207.
- [11] R. Hernández, R.L. Frederick, Spatial and thermal features of three dimensional Rayleigh–Bénard convection, *Int. J. Heat Mass Transfer* 37 (1994) 411–424.
- [12] D.D. Gray, A. Giorgini, The validity of the Boussinesq approximation for liquids and gasses, *Int. J. Heat Mass Transfer* 19 (1976) 545–551.
- [13] I. Cuesta, Estudi numèric de fluxos laminars i turbulents en una cavitat cúbica, PhD. thesis. Universitat Rovira i Virgili, Tarragona, Spain, 1993.
- [14] I. Cuesta, F.X. Grau, F. Giralt, Simulación numérica de flujos tridimensionales no estacionarios mediante el código de segundo orden 3DINAMICS, *An. Quím* 91 (1995) 655–665.
- [15] G. DeVahl Davis, I.P. Jones, Natural convection in a square cavity: a comparison exercise, *Int. J. Num. Meth. Fluid* 3 (1983) 227–248.
- [16] A. Belmonte, A. Tegner, A. Libchaber, Temperature and velocity boundary layers in turbulent convection, *Phys. Rev. E* 50 (1994) 269–279.
- [17] J.P. Gollub, S.V. Benson, Many routes to turbulent convection, *J. Fluid Mech* 100 (1980) 449–470.
- [18] D. Mukutmoni, K.T. Yang, Rayleigh–Bénard convection

- in a small aspect ratio enclosure: Part I Bifurcation to oscillatory convection, *J. Heat Transfer* 115 (1993) 360–366.
- [19] E.L. Koschmieder, *Bénard Cells and Taylor Vortices*, 1st ed. Cambridge Monographs on Mechanics and Applied Mathematics, Cambridge University Press, Cambridge, 1993.
- [20] F.H. Busse, R.M. Clever, Instabilities of convection rolls in a fluid of moderate Prandtl number, *J Fluid Mechanics* 91 (1979) 319–335.
- [21] R.J. Moffat, Personal communication, 1996.
- [22] G.D. Raithby, K.G.T. Hollands, in: W. Rohsenow, J. Hartnett, E. Ganic (Eds.), *Handbook of heat transfer fundamentals*. McGraw-Hill, New York, 1985.
- [23] J.P. Holman, *Heat Transfer*, 4th ed., McGraw-Hill, Tokyo, 1976, p. 258.